ORIGINAL ARTICLE

Suppression of non-small-cell lung cancer A549 tumor growth by an mtDNA mutation-targeting pyrrole-imidazole polyamide-triphenylphosphonium and a senolytic drug

Kohei Tsuji[1] | Yuki Kida[1] | Nobuko Koshikawa[1] | Seigi Yamamoto[1] |
Yoshinao Shinozaki[1] | Takayoshi Watanabe[2] | Jason Lin[1] [iD] | Hiroki Nagase[1] [iD] |
Keizo Takenaga[1] [iD]

[1]Division of Cancer Genetics, Chiba Cancer Center Research Institute, Chiba, Japan

[2]Division of Innovative Cancer Therapeutics, Chiba Cancer Center Research Institute, Chiba, Japan

Correspondence
Keizo Takenaga, Division of Cancer Genetics, Chiba Cancer Center Research Institute, 666-2 Nitona-cho, Chuoh-ku, Chiba 260-8717, Japan.
Email: ktakenaga@chiba-cc.jp

Present address
Yoshinao Shinozaki, Organometallchemie Eduard-Zintl-Institut, Technische Universität Darmstadt, Darmstadt, Germany

Funding information
Japan Society for the Promotion of Science KAKENHI, Grant/Award Number: 19K07654, JP26290060, 17H03602, JP16H01579 and JP20H03540; AMED, Grant/Award Number: 18ae0101051, 21zf0127001h0001 and 21ek0109495h0001

Abstract

Certain somatic mutations in mtDNA were associated with tumor progression and frequently found in a homoplasmic state. We recently reported that pyrrole-imidazole polyamide conjugated with the mitochondria-delivering moiety triphenylphosphonium (PIP-TPP) targeting an mtDNA mutation efficiently induced apoptosis in cancer cells with the mutation but not normal cells. Here, we synthesized the novel PIP-TPP, CCC-021-TPP, targeting *ND6* 14582A > G homoplasmic missense mutation that is suggested to enhance metastasis of non-small-cell lung cancer A549 cells. CCC-021-TPP did not induce apoptosis but caused cellular senescence in the cells, accompanied by a significant induction of antiapoptotic BCL-XL. Simultaneous treatment of A549 cells with CCC-021-TPP and the BCL-XL selective inhibitor A-1155463 resulted in apoptosis induction. Importantly, the combination induced apoptosis and suppressed tumor growth in an A549 xenografted model. These results highlight the potential of anticancer therapy with PIP-TPPs targeting mtDNA mutations to induce cell death even in apoptosis-resistant cancer cells when combined with senolytics.

KEYWORDS
apoptosis, mitochondria, mtDNA, mutation, pyrrole-imidazole polyamide

1 | INTRODUCTION

Pyrrole-imidazole polyamide is a functional molecule created by mimicking the DNA sequence recognition mechanism of the antibiotics distamycin A, netropsin, and duocarmycin.[1] Pyrrole-imidazole polyamide is composed of Py and Im and has the property of binding to the minor groove of B-type DNA in a base sequence-specific manner.[2–4] The Py/Py pair recognizes adenine (A)/thymine (T) and T/A base pairs, and Py/Im and Im/Py pair recognize cytosine (C)/guanine (G) and G/C base pairs, respectively, according to Dervan's rule.[4] With a combination of Py and

---

Im so as to recognize the DNA base sequence of an arbitrary gene or promoter region, it is possible to suppress the expression of a target gene.[2–4] Furthermore, PIPs can be conjugated with various functional moieties such as the alkylating agent *seco*-CBI and mitochondria-homing moiety TPP lipophilic cation at either the N- or C-terminus.[5–8] So far, our laboratory has reported that several PIPs-*seco*-CBI show anticancer effects.[5–7]

It has been reported that mitochondrial dysfunction is responsible for not only many disorders inducing neurodegenerative diseases and mitochondrial diseases but also tumorigenesis and metastasis.[9–11] Mitochondrion has its own genome called mtDNA that is a double-stranded circular DNA of 16,569 bp in length.[12] In previous studies, we reported that some somatic mtDNA mutations such as *ND6* 13997G > A mutation and *ND6* 13885insC mutation enhanced cancer metastasis,[13–15] that lymphomas and diabetes are caused by a mtDNA etiological mutation in mice,[16] and that some *ND* gene somatic mutations are homoplasmic in the primary and metastatic tissues of NSCLC and colon cancers.[14] Other laboratories also reported invasion/metastasis-enhancing potential of several mtDNA mutations in a variety of cancers.[17–22] These reports suggest that mtDNA homoplasmic mutations or single nucleotide variants could be promising targets for discovery of novel anticancer agents. Thus far, although many drugs targeting mitochondria have been developed,[23] few agents directly targeting mtDNA mutations are available. To explore this issue, we have recently evolved a strategy using PIP-TPPs, CCC-018-TPP and CCC-020-TPP, targeting homoplasmic 3243A > G mutation to induce apoptosis in cancer cells harboring the mutation.[8,24] One of the advantages of this strategy is that PIP-TPPs target mtDNA mutants, leaving WT mtDNA virtually intact.

In the present study, to assess the generality of anticancer effects of PIP-TPP, we synthesized the novel linear five-ring PIP-TPP, CCC-021-TPP, targeting *ND6* 14582A > G missense mutation that is reported to enhance metastasis of NSCLC A549 cells.[25] Here, we show that CCC-021-TPP did not induce apoptosis in A549 cells but provoked cellular senescence, and the combination of CCC-021-TPP with BCL-2 family inhibitors activated the apoptotic cell death program in vitro and in vivo, without apparent effects on cells with WT mtDNA sequence. Considering that PIP-TPPs can be designed in principle to any cancer-specific mtDNA mutations, these results indicate that PIP-TPPs targeting mtDNA mutations serve as therapeutics against certain apoptosis-resistant cancers as well as apoptosis-prone cancers.

2 | MATERIALS AND METHODS

2.1 | Reagents

Bafilomycin A1 was obtained from Sigma-Aldrich. ABT-199, ABT-263, and A-1155463 were purchased from Cayman Chemical.

2.2 | Cells and cell culture

Human NSCLC cell lines A549, PC-14, and Lu99 were used in this study. The authenticity of A549 and Lu99 cells was confirmed by STR DNA profile analysis undertaken by BEX Co. Ltd (Figure S1). PC-14

cells have been maintained in our institute since 1986,[26] and the STR profile of the cell line is different from the PC-14 cell line that was originally deposited with Riken BioResource Center in 1989 and subsequently shown to be identical to PC-9 cell line (https://web.expasy.org/cellosaurus/CVCL_1640) (Figure S1). A549 cells but not PC-14 or Lu99 cells harbor homoplasmic 15582A > G mutation in the *ND6* gene (Figure S2A). A549 and Lu99 cells have WT p53 (https://web.expasy.org/cellosaurus/CVCL_0023 or https://web.expasy.org/cellosaurus/CVCL_3015, respectively), whereas PC-14 cells carry p53-R248W (c.742C > T) mutant (Figure S2B), which is different from R248Q (c.743G > A) mutant found in PC-9 cells (https://web.expasy.org/cellosaurus/CVCL_B260). Human dermal fibroblasts were obtained from Cell Applications, Inc. They were routinely cultured in DMEM-high glucose supplemented with 10% (v/v) FBS and 1% (v/v) penicillin/streptomycin (Gibco) in a humidified atmosphere with 21% O_2/5% CO_2 at 37°C.

2.3 | Synthesis of CCC-021-TPP

The liner 5-ring PIP (CCC-021) was synthesized using a PSSM-8 peptide synthesizer (Shimadzu), and conjugated with TPP at the N-terminus (Figure S3A), essentially as described previously.[8] The synthesized products were purified by HPLC (Shimadzu) and checked for purity by liquid chromatography/mass spectrometry (Shimadzu) (Figure S3B).

2.4 | Melting temperature shift assay

Melting temperature shift analysis using oligonucleotides representing CCC-021-TPP binding regions within ND6-14582G ("Matched"; sense, 5′-CGGAATGCTAACTC-3′; antisense, 5′-GAGTTAGCATTCCG-3′) and ND6-14582A ("Mismatched"; sense, 5′-CGGAATACTAACTC-3′; antisense, 5′-GAGTTAGTATTCCG-3′) was carried out as previously described[24] with 10 μM CCC-021-TPP and minor changes in the hybridization process (CCC-021-TPP and duplex oligonucleotides were mixed and incubated at 30°C prior to analysis) and the thermal profile (denaturation profiles were recorded from 15°C to 80°C).

2.5 | Analysis of CCC-021-TPP localization in mitochondria

CCC-021-TPP localization in A549 cells was examined by using MitoTracker Red CMXRos (Thermo Fisher Scientific) and rabbit anti-TPP polyclonal Ab as described previously.[8,24]

2.6 | Measurement of respiratory chain complex I activity

Measurement of complex I activity was undertaken with the Complex I Enzyme Activity Microplate Assay Kit (Abcam) according to the manufacturer's instructions.

2.7 | Cell growth assay

A549 (250 cells/well) and PC-14 (500 cells/well) cells in 0.1 mL growth medium were seeded into a 96-well plate and incubated overnight. After treatment with DMSO or CCC-021-TPP, 10 μL MTT solution (5 mg/mL) was added to each well and incubated for 3.5 hours. Absorbance was measured at 470 nm using a microplate reader.

2.8 | Cell viability assay

Cell viability was assessed by Trypan blue dye exclusion test.

2.9 | Measurement of mtROS generation

For detection of mtROS, the cells were incubated with 25 nM MitoSOX Red (Thermo Fisher Scientific) at 37°C for 10 minutes.[8] Images were obtained on a confocal laser microscope; and per-cell fluorescence intensity was calculated using pixel values in ImageJ, version 1.53a.

2.10 | Mitophagy detection assays

Mitophagy was detected with a Mitophagy Detection Kit (Dojindo) according to the manufacturer's protocol; Mtphagy Dye emitted markedly red fluorescence upon the fusion of damaged mitochondria to lysosome (labeled by LysoDye, which emitted green fluorescence); images were obtained by confocal laser scanning microscopy, with the per-cell ratio of mitophagy determined in ImageJ. In another experiment, A549 cells were transfected with the pCMX-SAH/Y145F-LC3 plasmid expressing GFP-LC3 fusion proteins,[27] and then treated with DMSO or CCC-021-TPP. The cells were stained with 100 nM MitoTracker Red for 10 minutes and then observed under a confocal laser scanning microscope.

2.11 | Senescence-associated β-galactosidase staining

Senescence-associated β-galactosidase staining was performed with a SPiDER-β-Gal Staining Kit (Dojindo). Images were obtained using a confocal laser scanning microscope.

2.12 | RNA isolation and real-time quantitative PCR

mRNA isolation, reverse transcription, and quantitative PCR were carried out as described previously.[15] The mRNA expression level was normalized to that of 18S ribosomal RNA (RPS18). The forward and reverse primers used are summarized in Table S1.

2.13 | Western blot analysis

Protein sample preparation, SDS-PAGE, and western blotting were carried out as described previously.[15] The primary Abs are summarized in Table S2; membranes were scanned by a Lumino Imaging Analyzer (GE Healthcare), and ImageJ was used to normalize the signal intensity for each protein to that of β-actin.

2.14 | Enzyme-linked immunosorbent assay

A549 and PC-14 cells were seeded at a concentration of 250 or 500 cells per well, respectively, in a 96-well plate in 0.1 mL of DMEM/10% FBS. The next day, DMSO or CCC-021-TPP was added. After incubation for 4 days, the medium was changed to 0.1 mL of fresh DMEM/10%FBS, and conditioned media were harvested after 24 hours of cultivation. Cells were lysed in RIPA buffer, and the protein concentration was measured by the BCA method using BSA as a standard. Human IL-6 and IL-8 concentrations were measured with the Human IL-6 ELISA Kit (BioLegend) and the Human IL-8 ELISA Kit (Proteintech), respectively, according to the manufacturers' instructions and expressed as ng/mg protein.

2.15 | Annexin V/PI staining

Annexin V staining was carried out with the MEBCYTO Apoptosis Kit (MBL). Stained cells were analyzed by flow cytometer BD FACSCaliber and FlowJo Software (Becton Dickinson).

2.16 | Cell cycle analysis

The cells were harvested with 0.05% trypsin, fixed with 70% ethanol, and stored at −20°C until use. The cells were incubated in PCB (192 mM Na_2HPO_4/16 mM citric acid) for 15 minutes at room temperature. They were then centrifuged, resuspended in PI-RNase solution (50 μg/mL PI/100 μg/mL RNase A/PBS) and incubated for 30 minutes at room temperature. Stained cells were analyzed by a flow cytometer (BD FACSCaliber) and the data were analyzed using FlowJo Software.

2.17 | Animal experiments

The animal experiments were approved by the Committee on the Ethics of Animal Experiments of Chiba Cancer Center (Permission Number: 18-1) and carried out in compliance with the institutional guidelines for the care and use of animal research and the ARRIVE Guidelines 2.0.[28] A549 cells (2×10^6) were injected subcutaneously into 4-week-old female nude mice (Charles River Laboratories Japan). When the average tumor size reached approximately 80 mm^3, the mice were randomized into four groups. Mice in the control group ($n = 5$) received vehicle alone (2% DMSO/30%

PEG300/2% Tween-80/PBS). Mice in the CCC-021-TPP group ($n = 5$) and the A-1155463 group ($n = 5$) were intraperitoneally treated with CCC-021-TPP (5 mg/kg body weight) twice a week and A-1155463 (5 mg/kg body weight) daily, respectively. Mice in the combination group ($n = 5$) were injected with CCC-021-TPP and A-1155463 twice a week and daily, respectively. Tumor volume was estimated from the equation of $a \times b^2/2$,
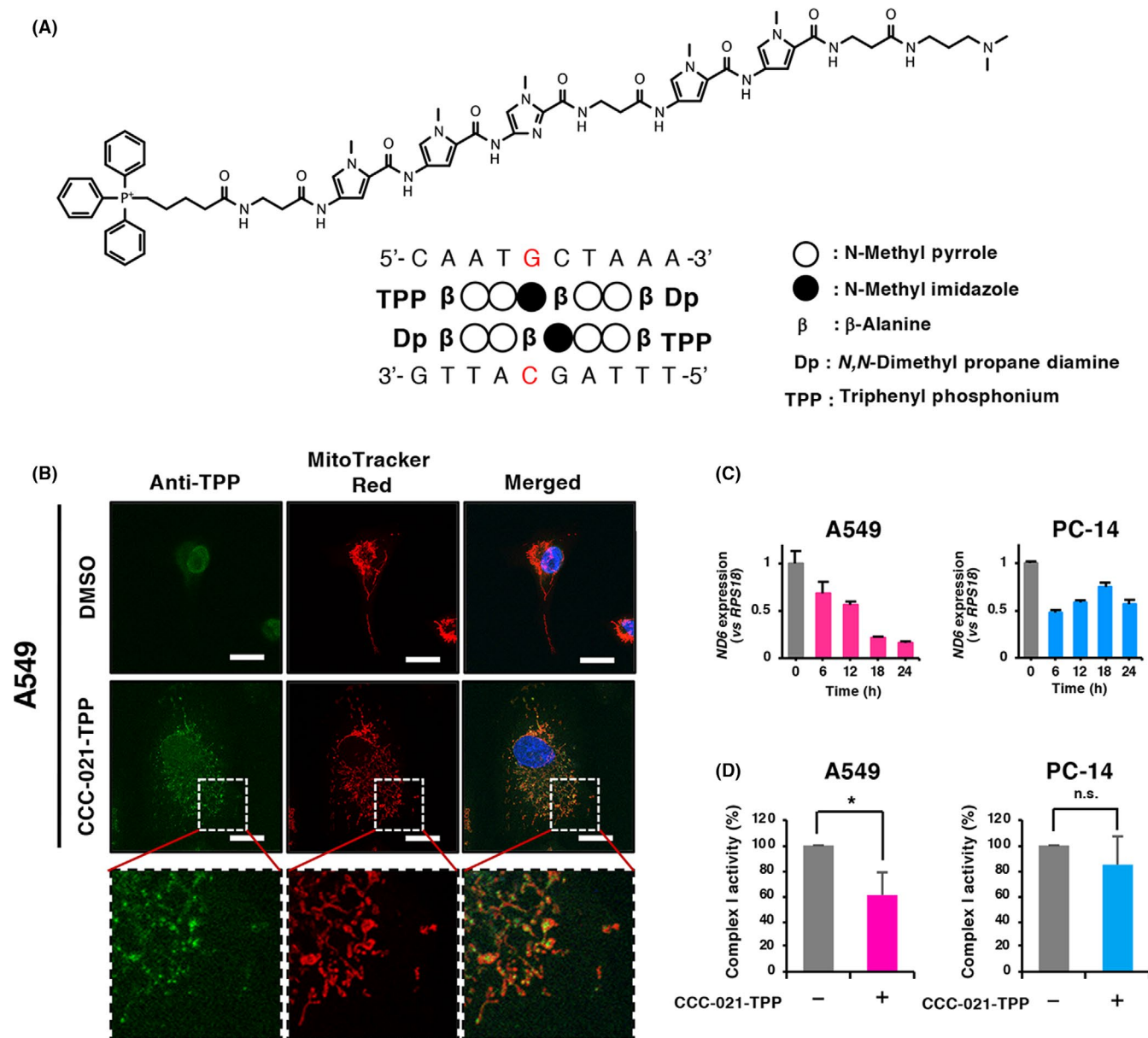

FIGURE 1 Chemical formula and specificity of CCC-021-triphenylphosphonium (TPP). (A) Chemical structure of CCC-021-TPP and its predicted binding mode to the target sequence. Bases in red indicate mutated bases. (B) Representative images of mitochondria stained with anti-TPP Ab (AF488) and MitoTracker Red in A549 cells treated with DMSO or 20 μM CCC-021-TPP for 24 h. Bar = 20 μm. (C) Expression of the *ND6* gene in A549 and PC-14 cells cultured with CCC-021-TPP. Cells were treated with 20 μM CCC-021 for the indicated times. (D) Complex I enzyme activity in CCC-021-TPP-treated A549 and PC-14 cells. Cells were treated with DMSO or 10 μM CCC-021-TPP for 24 h. Values are mean ± SD (n = 4). *$P < .05$ vs DMSO control. n.s., not significant (Student's *t* test)

FIGURE 2 Increases in mitochondrial reactive oxygen species (ROS) production and mitophagy in CCC-021-triphenylphosphonium (TPP)-treated A549 cells. (A) Mitochondrial ROS production in A549 and PC-14 cells treated with DMSO or 10 μM CCC-021-TPP for 24 h; FI, fluorescence intensity, as indicated on the right (A549, n = 32:35 DMSO : CCC-021-TPP; PC-14, n = 22:48 DMSO : CCC-021-TPP). Scale bar = 30 μm. (B) Mitophagy detection in A549 and PC-14 cells; ratio of Mtphagy Dye and Lyso Dye per-cell fluorescence intensity shown on the right (A549, n = 45:14 DMSO : CCC-021-TPP; PC-14, n = 15:15 DMSO : CCC-021-TPP). n.s., not significant. (C) Mitophagy detection in living A549 cells expressing GFP-LC3. Cells were treated with DMSO or 20 μM CCC-021-TPP for 3 d. Bar = 20 μm. (D) Western blot analysis of the expression of LC3 in A549 cells treated with bafilomycin A1 (Baf) at indicated concentrations. Uncropped western blot images are shown in Figure S12
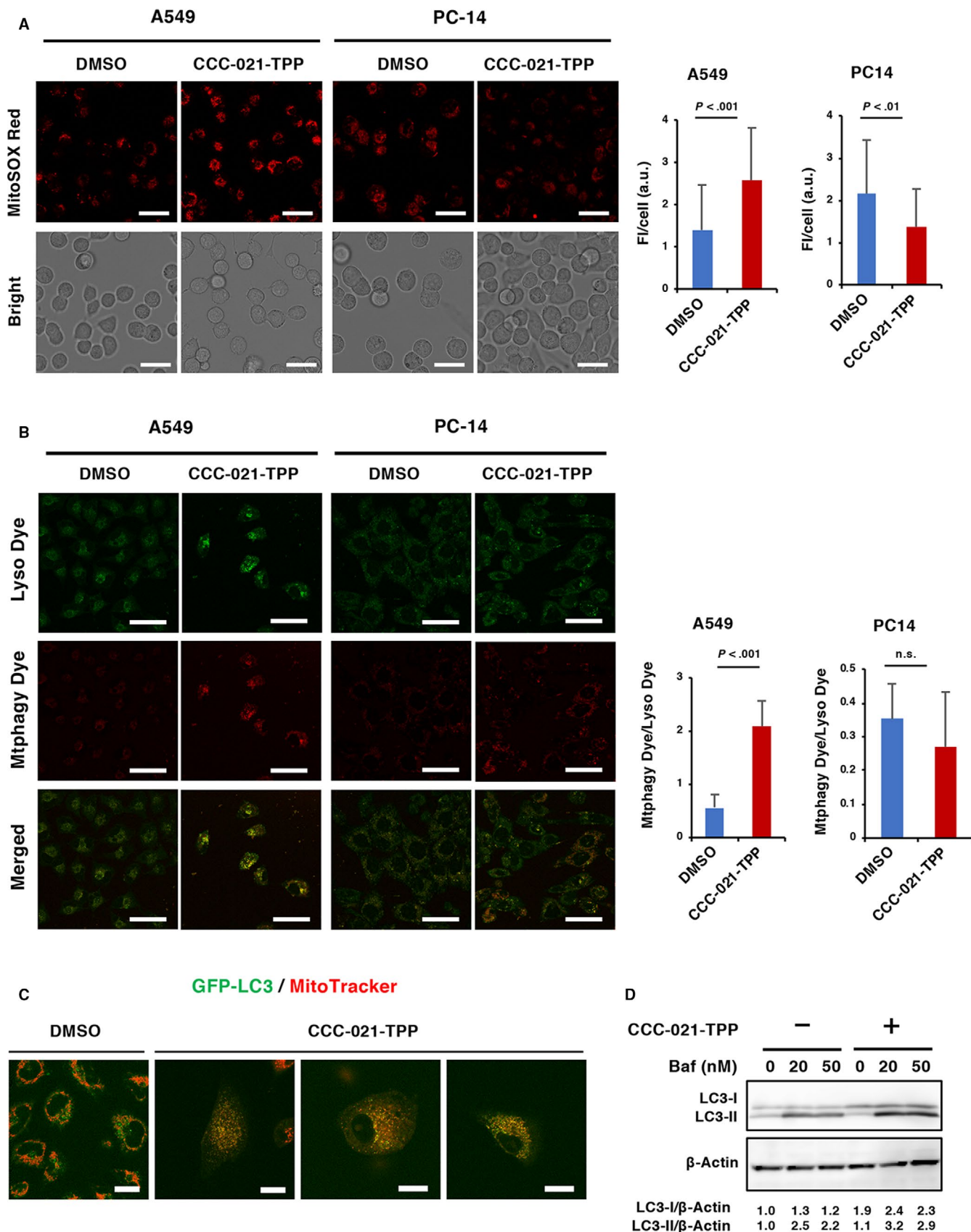
where a and b represent long and short diameter, respectively. On day 21, the mice were killed by carbon dioxide for approximately 15 minutes after respiratory arrest to ensure minimal suffering. Tumor tissues were removed and subjected to histochemical analyses.

2.18 | Histochemical analyses

Tumor and several organ tissues were fixed with 4% paraformaldehyde, embedded in paraffin, and then cut into 5-μm sections. The tissues were

deparaffinized and used for H&E staining and histochemical analyses. For detection of TPP or F4/80, after heat-induced antigen retrieval in DAKO REAL Target Retrieval Solution (Agilent Technologies), the tissues were treated with 5% dry milk/1% goat serum/PBS to block non-specific binding sites, and then immunofluorescent staining was carried out with rabbit polyclonal anti-TPP Ab and Alexa Fluor 594 (AF594)- or AF488-conjugated goat anti-rabbit IgG (Thermo Fisher Scientific) or PE anti-mouse F4/80 Ab (BioLegend). After treating with Vector True VIEW Auto Fluorescence Quenching Kit (Vector Laboratories) for 5 minutes, the tissue sections were mounted with VECTASHIELD (Vector Laboratories). For TUNEL assay, deparaffinized tissues were stained with MEBSTAIN Apoptosis TUNEL Kit Direct (MBL) and counterstained with DAPI. Senescence-associated β-galactosidase was stained with Senescence β-Galactosidase Staining Kit (Cell Signaling Technology) and the tissues were counterstained with Nuclear Fast Red. For immunohistochemistry, after heat-induced antigen retrieval and subsequent inactivation of endogenous peroxidase with 3% H_2O_2 in PBS and blocking, the tissues were incubated with primary Abs (Table S2). The antigens were detected with the avidin-biotin-peroxidase complex method using 3,3'-diaminobenzidine as a chromogen. The tissues were counterstained with Mayer's hematoxylin.

2.19 | Statistics

The data are presented as the mean ± SD of at least three determinations. The statistical significance was calculated using Student's *t* test or one-way ANOVA and Tukey's test. The significance level is set at a $P < .05$.

3 | RESULTS

3.1 | Specificity of CCC-021-TPP in targeting *ND6* 14582A > G mutation in A549 cells

We designed the PI polyamide CCC-021-TPP that was expected to bind to the target sequence containing 14582G mutation in an antiparallel fashion (Figures 1A). Thermal shift assay confirmed selective CCC-021-TPP binding by the measurable increase in the thermal stability of the matched 13-mer duplex DNA oligonucleotide ligand (14582A > G) compared to the mismatch (14582A) upon contact with CCC-021-TPP (Table S3). We examined the localization of CCC-021-TPP in A549 as well as other cells (PC-14, Lu99, and HDF) used in this study post-CCC-021-TPP treatment. CCC-021-TPP showed

clear mitochondrial localization (Figures 1B and S4), and significantly suppressed *ND6* gene expression in A549 cells, although the effect, while similar, was only slight in PC-14 (Figure 1C). Furthermore, CCC-021-TPP inhibited the respiratory chain complex I activity in A549 cells but not in PC-14 cells (Figure 1D). Together, these results ensured the specificity of CCC-021-TPP to the 14582G mutation.
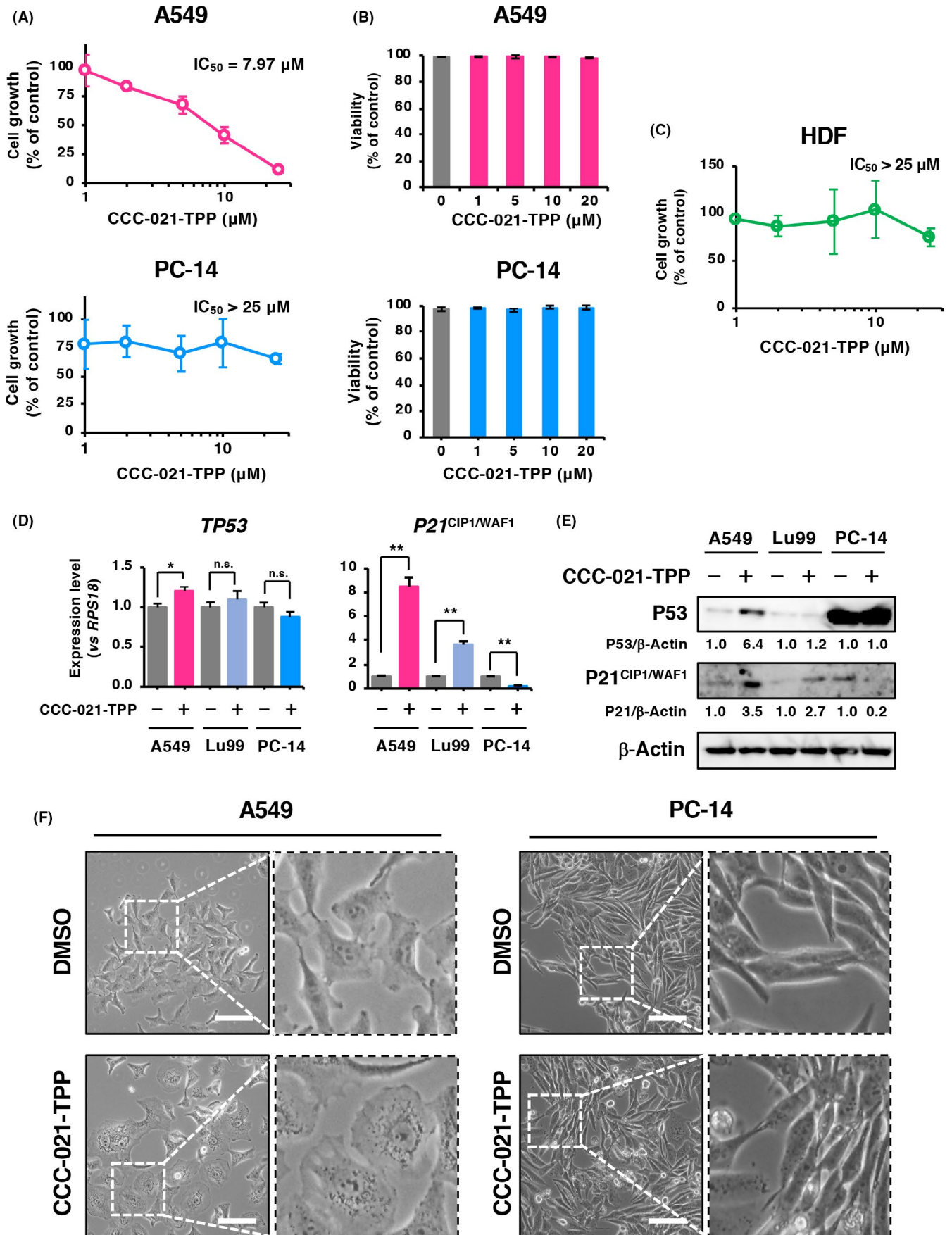
3.2 | CCC-021-TPP enhanced mtROS generation and induced mitophagy in A549 cells

We next investigated the effects of CCC-021-TPP on mitochondrial stress in A549 cells. MitoSOX Red staining indicated an increase in mtROS generation in A549 cells treated with CCC-021-TPP, but a decrease was observed in PC-14 cells (Figure 2A). As excessive mtROS production is known to damage the mitochondrial integrity and triggers the mitochondrial quality control mechanism mitophagy,[29] we checked the degree of mitophagy in CCC-021-TPP-treated A549 cells. We found a marked mitophagy induction in A549 cells but not in PC-14 cells after treatment with CCC-021-TPP (Figure 2B). We also confirmed mitophagy induction by examining colocalization of GFP-LC3 and MitoTracker Red in living cells; puncta of GFP-LC3 and mitochondria tended to localize separately in DMSO-treated cells while most of them colocalized in CCC-021-TPP-treated cells (Figure 2C). Western blot analysis revealed an increase in the autophagy marker LC3-II in CCC-021-TPP-treated A549 cells only in the presence of bafilomycin A1, an inhibitor of fusion between autophagosomes and lysosomes[30] (Figure 2D), suggesting a high turn-over rate of LC3-II in the cells. These data suggest that CCC-021-TPP caused mitochondrial stress in A549 cells.

3.3 | CCC-021-TPP suppresses cell growth and induces cell senescence in A549 cells

To determine whether CCC-021-TPP affects the phenotypes of A549 cells, cell growth and cell viability of CCC-021-TPP-treated cells were examined by MTT assay and Trypan blue dye exclusion test, respectively. We found that CCC-021-TPP suppressed cell growth of A549 cells in a dose-dependent manner (IC_{50} value, 7.97 μM) but not of PC-14 cells (IC_{50} value, >25 μM) and it did not affect cell viability at all (Figure 3A,B). CCC-021-TPP slightly suppressed the growth of HDF cells only at higher concentrations (Figure 3C), suggesting its low cytotoxicity

FIGURE 3 Induction of cell growth arrest but not cell death in CCC-021-triphenylphosphonium (TPP)-treated A549 cells. (A) MTT assay. A549 and PC-14 cells were treated with CCC-021-TPP at the indicated concentrations for 5 d. (B) Cell viability assay. A549 and PC-14 cells were cultured with DMSO or CCC-021-TPP at the indicated concentrations for 7 d. Cell viability was assayed by Trypan blue dye exclusion test. (C) MTT assay. HDF cells were treated with CCC-021-TPP at the indicated concentrations for 5 d. (D) Real time quantitative PCR analysis of the expression of *p53* and *p21*. Cells were cultured with DMSO or 20 μM CCC-021-TPP for 4 d. *RPS18* served as an internal control. Values are mean ± SD (*n* = 3). *$P < .05$, **$P < .01$ vs DMSO control. n.s., not significant (Student's *t* test). (E) Expression of p53 and p21 proteins. Cells were treated with DMSO or 20 μM CCC-021-TPP for 4 d. β-Actin served as a loading control. Uncropped western blot images are shown in Figure S12. (F) Cell morphology. Representative images of A549 and PC-14 cells treated with DMSO or 20 μM CCC-021-TPP for 5 d. Bar = 100 μm

(A) A549

Cell growth (% of control) vs CCC-021-TPP (μM)
IC$_{50}$ = 7.97 μM

PC-14

Cell growth (% of control) vs CCC-021-TPP (μM)
IC$_{50}$ > 25 μM

(B) A549

Viability (% of control) vs CCC-021-TPP (μM)

PC-14

Viability (% of control) vs CCC-021-TPP (μM)

(C) HDF

Cell growth (% of control) vs CCC-021-TPP (μM)
IC$_{50}$ > 25 μM

(D) *TP53*

Expression level (vs *RPS18*)
CCC-021-TPP − + − + − +
A549 Lu99 PC-14

P21$^{CIP1/WAF1}$

CCC-021-TPP − + − + − +
A549 Lu99 PC-14

(E)

	A549		Lu99		PC-14	
CCC-021-TPP	−	+	−	+	−	+
P53						
P53/β-Actin	1.0	6.4	1.0	1.2	1.0	1.0
P21$^{CIP1/WAF1}$						
P21/β-Actin	1.0	3.5	1.0	2.7	1.0	0.2
β-Actin						

(F) A549 / PC-14

DMSO / CCC-021-TPP

to normal cells. We observed a slight and a significant increase in *TP53* and *P21*[WAF1/CIP1] mRNA expression, respectively, in A549 cells but not in PC-14 cells treated with CCC-021-TPP (Figure 3D). Accordingly, CCC-021-TPP markedly enhanced P53 and P21[CIP1/WAF1] expressions at the protein level in A549 cells compared to PC-14 cells that express mutant P53 (Figure 3E). To exclude nonspecific activation of the P53-P21[CIP1/WAF1] pathway, we treated Lu99 cells that have WT p53 but do not harbor 14582G mutation with CCC-021-TPP, and observed only a slight increase in P21[CIP1/WAF1] but not P53, again indicating highly specific recognition of 14582G mutation by CCC-021-TPP (Figure 3D,E). Because A549 cells are deficient in the *CDKN2A* locus,[31] we did not examine the expression of the *P16*[INK4a] or *P14*[ARF] genes in the cell lines used in this study. Interestingly, microscopic observation revealed that CCC-021-TPP-treated A549 cells but not PC-14 cells became more flattened, enlarged, and granular in the cytoplasm compared to DMSO control (Figure 3F), resembling the morphology of senescent cells.

3.4 | CCC-021-TPP induced cellular senescence in A549 cells

Staining with SA-β-Gal showed an increase in the number of positive cells in A549 cells but not in PC-14 cells treated with CCC-012-TPP (Figure 4A). Consistent with the observation, CCC-021-TPP enhanced the production of the SASP factors including *IL1A*, *IL6*, and *IL8* mRNAs[32] in A549 cells compared to PC-14 cells (Figure 4B). The ELISA analyses confirmed the enhanced secretion of IL-6 and IL-8 in A549 cells but not in PC-14 cells treated with CCC-021-TPP (Figure 4C). These results convincingly indicated that CCC-021-TPP specifically induced cellular senescence in A549 cells.

Treatment of A549 cells with CCC-021-NH$_2$ that would localize mainly in the nucleus but barely in mitochondria showed a very weak activity in inducing morphological change and IL-6 secretion in A549 cells compared to CCC-021-TPP (Figure S5), indicating that mitochondrial localization of CCC-021-TPP is important for inducing cellular senescence. In addition, simultaneous treatment of A549 cells with CCC-021-TPP and the autophagy/mitophagy inhibitor 3-MA[33,34] suppressed the induction of cellular senescence (Figure S6), suggesting the importance of autophagy/mitophagy in inducing cellular senescence.

3.5 | CCC-021-TPP enhanced BCLXL expression in A549 cells

To obtain clues about the reason why CCC-021-TPP did not induce apoptosis, we checked the expression level of apoptosis-related genes by real-time quantitative PCR and western blot analysis. Consequently, we found that the expression of the proapoptotic BAX was increased while those of the antiapoptotic BCL2, BCLW, SURVIVIN, and MCL1 were decreased in CCC-021-TPP-treated A549 cells compared to CCC-021-TPP-treated PC-14 cells, seemingly the cells being inclined toward apoptosis. However, an obvious increase in the expression of the antiapoptotic BCLXL was observed in CCC-021-TPP-treated A549 cells (Figure 5).

3.6 | Combination with CCC-021-TPP and BCL-XL selective inhibitor induced apoptosis in A549 cells

To examine the role of enhanced BCL-XL expression in CCC-021-TPP-treated A549 cells, we simultaneously treated the cells with CCC-021-TPP and the BCL-2 inhibitor ABT-199, the BCL-2 family inhibitor ABT-263 or the BCL-XL inhibitor A-1155463. The MTT assay showed that the combination of a low dose of CCC-021-TPP and ABT-263 or A-1155463 synergistically reduced cell survival of A549 cells but not of PC-14 cells (Figures 6A and S7A). In contrast, the combination of CCC-021-TPP and ABT-119 failed to do so (Figure 6B). The combination of CCC-021-TPP and A-1155463 or ABT-263 induced apoptosis-like morphological change, such as membrane blebbing, in A549 cells but not in PC-14 cells (Figures 6C and S7B). Actually, the levels of apoptosis-related markers such as cleaved poly(ADP-ribose) polymerase-1 (PARP-1), CC3, and γ-H2AX, and the number of cells positive for annexin V and cells in the sub-G$_1$ fraction were increased after the combined treatment only in A549 cells (Figure 7). These results indicated that inhibition of BCL-XL in CCC-021-TPP-treated A549 cells can induce apoptosis.

3.7 | Antitumor activity of combined CCC-021-TPP and A-1155463 treatment against A549 tumors

Based on the above results, we examined antitumor activity of the combination of CCC-021-TPP and A-1155463 against A549 xenografted tumors. To this end, we intraperitoneally administered either CCC-021-TPP or A-1155463 or both. As shown in Figure 8, we observed a clear trend toward the suppression of tumor growth in the mice given both agents, although statistically not significant (DMSO vs combination on day 21, $P = .0565$, one-way ANOVA). Treatment with CCC-021-TPP alone but not A-1155463 alone slightly suppressed tumor growth. Body weight loss was not observed in any group (Figure 8A). Histochemical analyses of tumor tissues revealed that CCC-021-TPP was detected in the cytoplasm of tumor cells as

---

FIGURE 4 Induction of cellular senescence in CCC-021-triphenylphosphonium (TPP)-treated A549 cells. (A) Induction of senescence-associated β-galactosidase (SA-β-Gal). A549 and PC-14 cells were treated with DMSO or 20 μM CCC-021-TPP for 5 d. Left panels: representative images of SA-β-Gal staining. Bar = 40 μm. Right panels: percentage of SA-β-Gal positive cells. N.D., not detected. (B) Expression of senescence-associated secretory phenotype genes. Cells were treated with DMSO or 20 μM CCC-021-TPP for 4 d. (C) Secretion of interleukin-6 (IL-6) and IL-8. Cells were treated with DMSO or 20 μM CCC-021-TPP for 4 d. Values are mean ± SD ($n = 3$). *$P < .05$, **$P < .01$, ***$P < .001$ vs DMSO control. n.s., not significant (Student's *t* test)
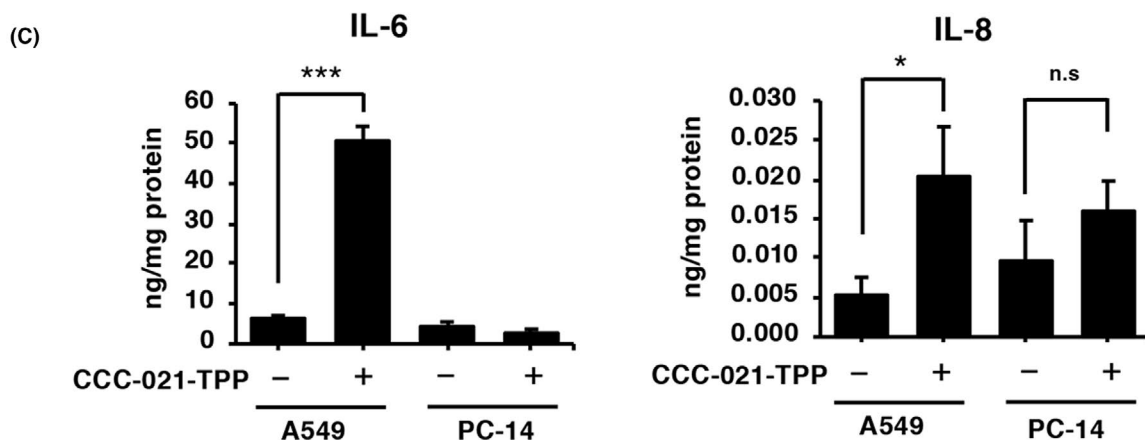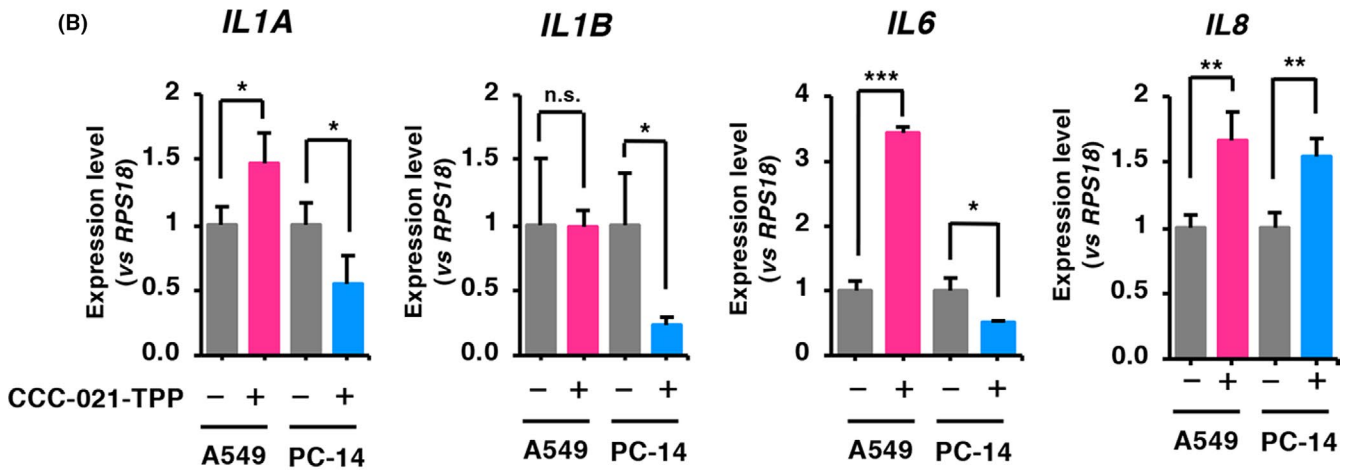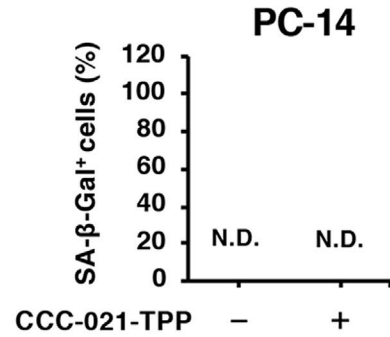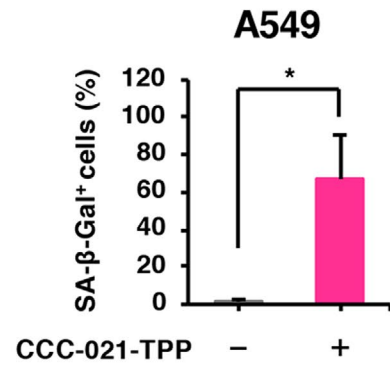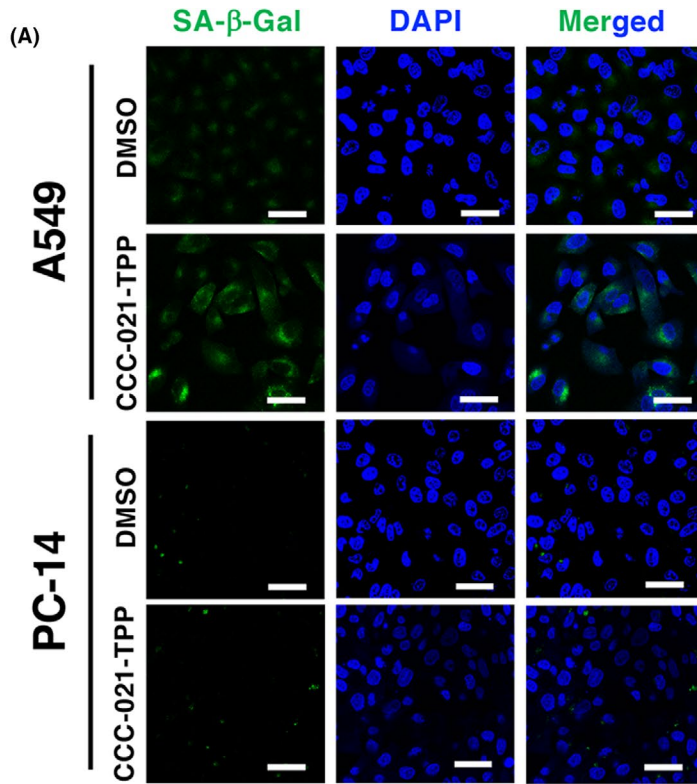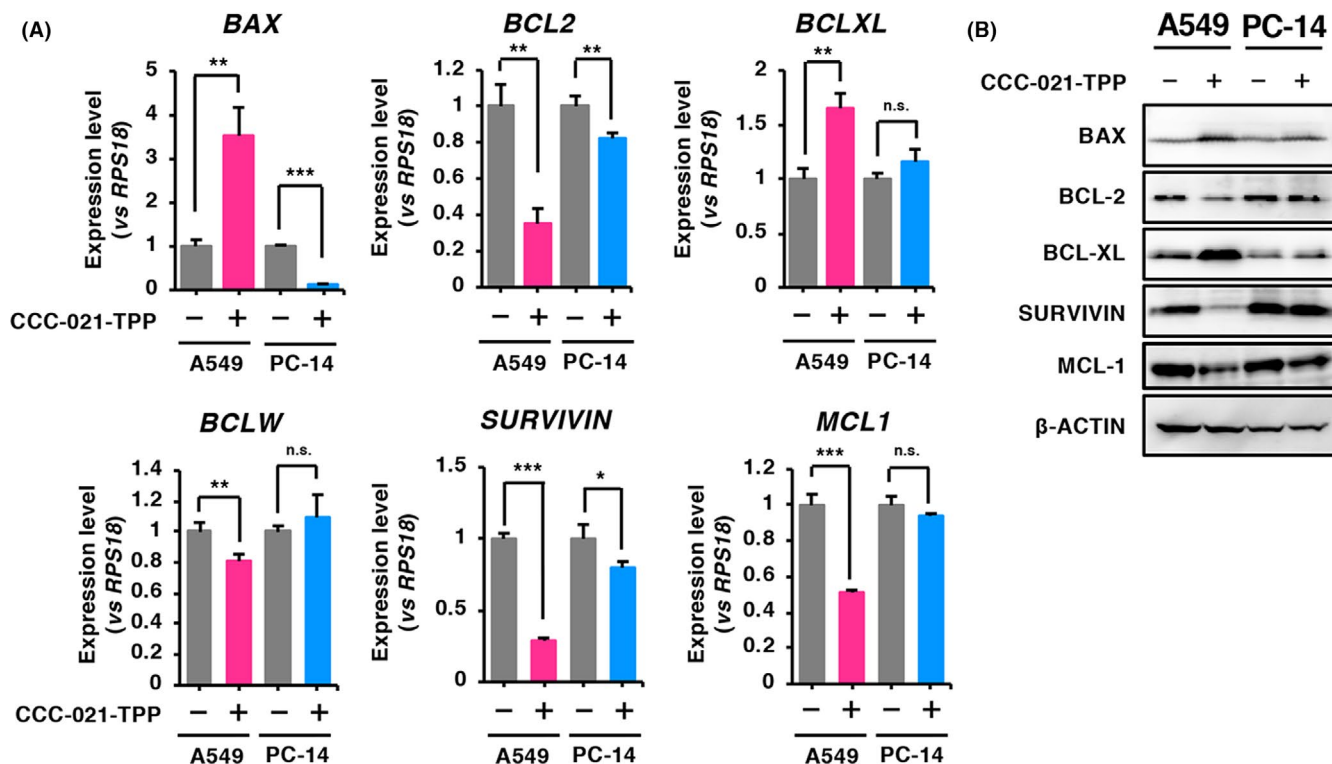
FIGURE 5 Expression of apoptosis-related genes in CCC-021-triphenylphosphonium (TPP)-treated A549 cells. (A) Expression of apoptosis-related genes. Cells were treated with DMSO or 20 μM CCC-021-TPP for 4 d. Values are mean ± SD (n = 3). *P < .05, **P < .01, ***P < .001 vs DMSO control. n.s., not significant (Student's t test). (B) Expression of apoptosis-related proteins. Cells were treated with DMSO or 20 μM CCC-021-TPP for 5 d. β-Actin served as a loading control. Uncropped western blot images are shown in Figure S12

assessed by TPP immunostaining (Figure 8B). Staining with H&E showed a somewhat altered morphology of tumor cells and tissue architecture in both the CCC-021-TPP-treated group and the combination group compared to those in other groups (Figure 8C). Interestingly, MPO-positive neutrophils accumulated in the CCC-021-TPP-treated group and the combination group (Figure 8C,D). The number of SA-β-Gal-positive cells increased in both the CCC-021-TPP-treated and the combination groups, indicating that cellular senescence was also induced by CCC-021-TPP in vivo. The number of cells expressing Ki-67, a marker of proliferating cells, slightly and significantly reduced in the CCC-021-TPP-treated group and the combination group, respectively. Apoptosis was clearly induced in the combination group as indicated by TUNEL staining (Figure 8C,D). Pan-cytokeratin and CC3 immunostainings also suggested a decrease in the number of tumor cells and an increase in apoptosis, respectively, in the combination group (Figure S8). However, the numbers of CD68+ macrophages and CD31+ tumor microvessels were not different among the groups (Figure S7). Together, it appeared that CCC-021-TPP induced cellular senescence and the

combination of CCC-021-TPP and A-1155463 caused apoptosis of A549 cells in vivo.

Following the lack of apparent body weight loss in this experiment, we further checked for other signs of possible toxicity of CCC-021-TPP in the treated mice by examining the end-point tissue distribution of the polyamide, local tissue architecture, as well as CC3 positivity in organs including brain, lung, liver, and kidney. We found CCC-021-TPP to be distributed in the lung, liver. and kidney, but not the brain (Figure S9A). The strong TPP immunostaining of Kupffer cells, which were double positive for TPP and F4/80 (Figure S9B) compared to parenchymal cells in the liver, was also noteworthy. Cleaved caspase-3 immunostaining of the CCC-021-TPP-accumulated organ tissues was negative for lung, hepatic parenchymal, and Kupffer cells, while a slight staining of tubular epithelium but not glomerular cells in the kidney was observed (Figure S10). The H&E staining showed no apparent tissue damage in any of the tissues examined (Figure S11), together suggesting that CCC-021-TPP did not cause severe adverse events in mice.

FIGURE 6 Combined effect of CCC-021-triphenylphosphonium (TPP) and A-1155463 or ABT-199 on cell survival of A549 cells. (A, B) Cell survival. Cells were treated with DMSO, 20 μM CCC-021-TPP alone, A-1155463, or ABT199 alone at the indicated concentrations, or the combination of 20 μM CCC-021-TPP and the indicated concentrations of the inhibitor for 4 d. Cell survival was measured with MTT assay. Each point represents mean ± SD (n = 3). (C) Representative images of cell morphology of cells treated with DMSO, 20 μM CCC-021-TPP alone, 10 μM A-1155463, or ABT-199 alone, or their combination for 4 d. Bar = 100 μm
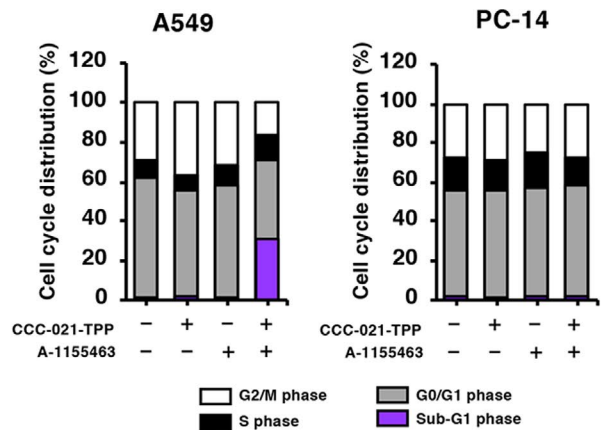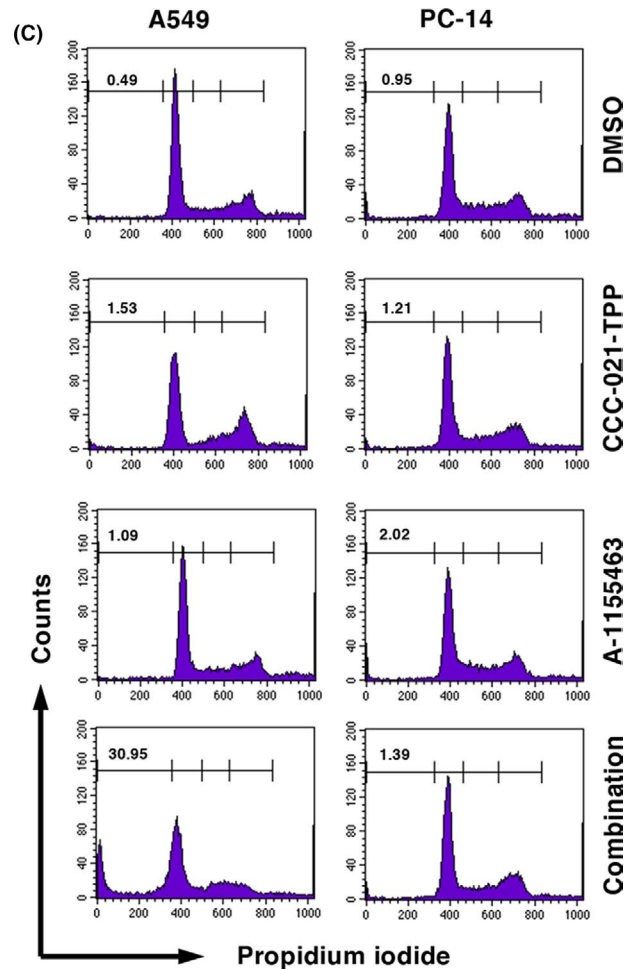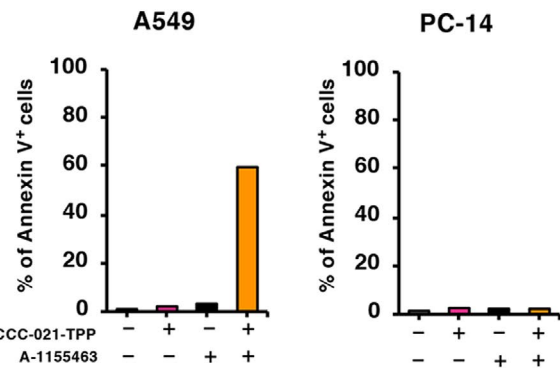
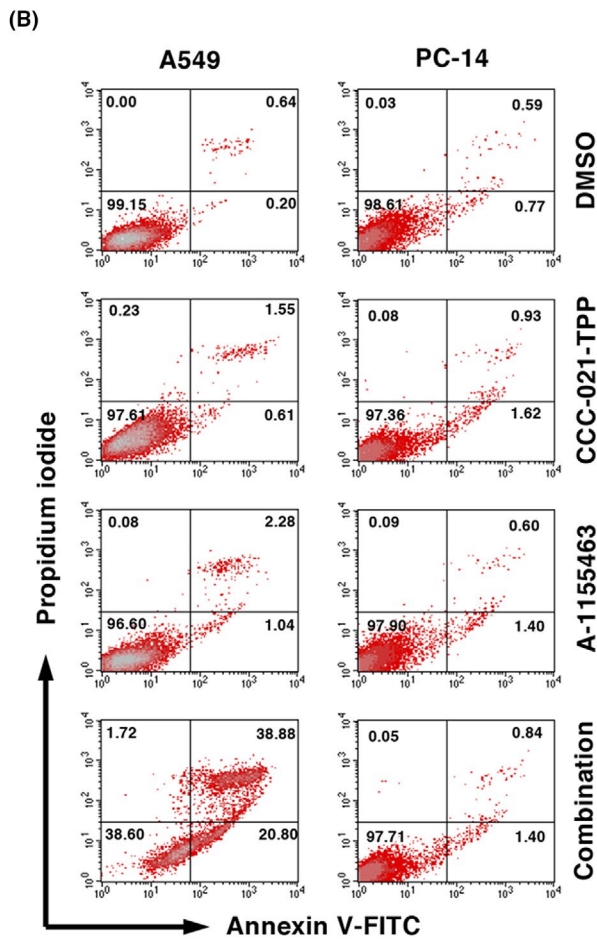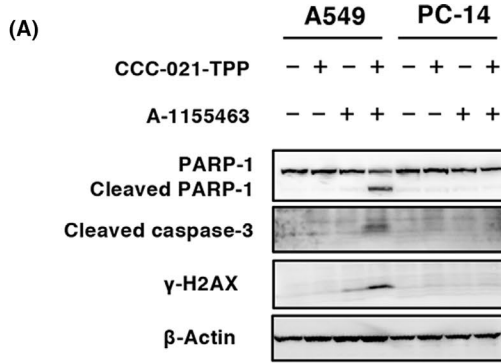**(A)**

(B)

(C)
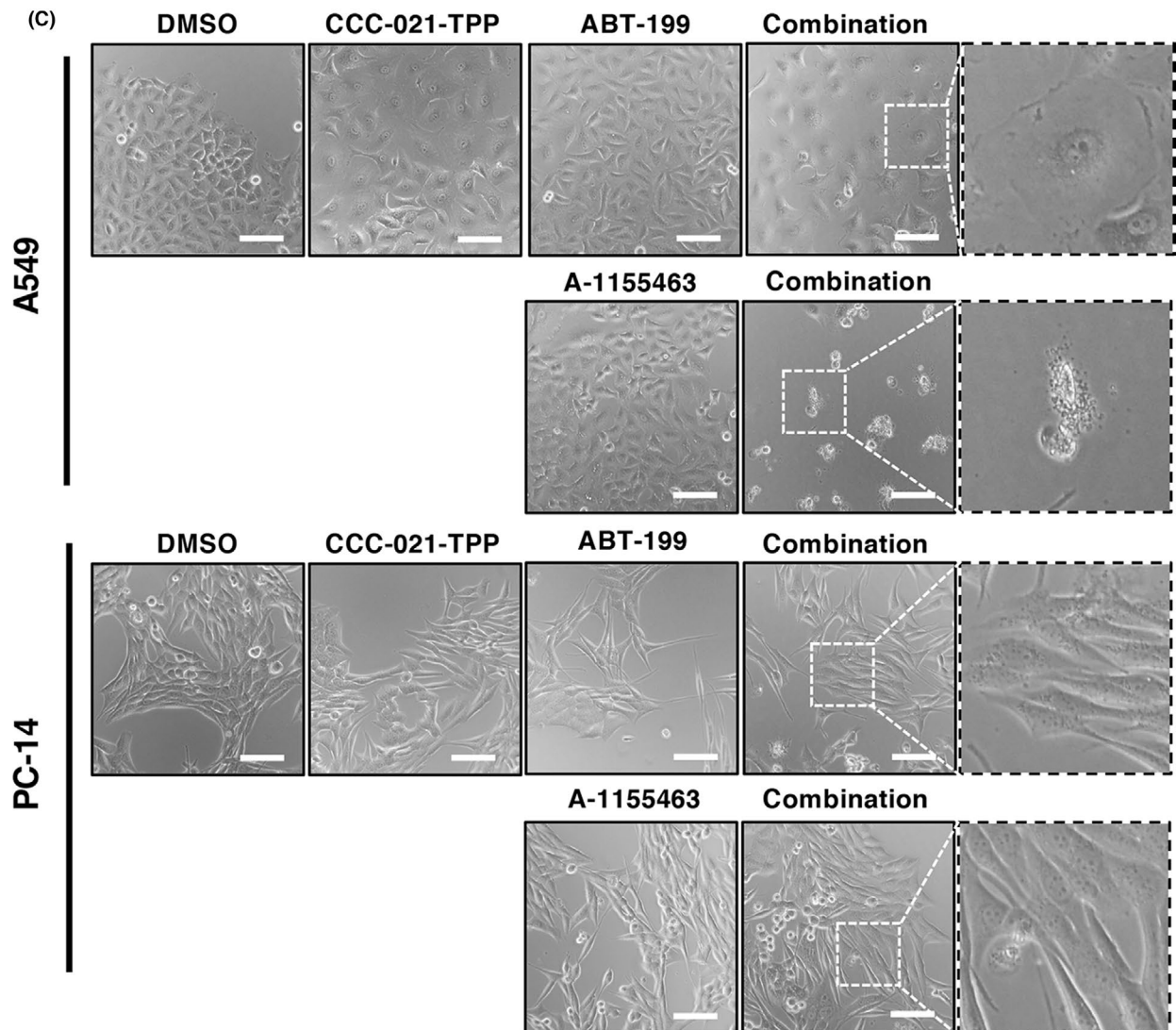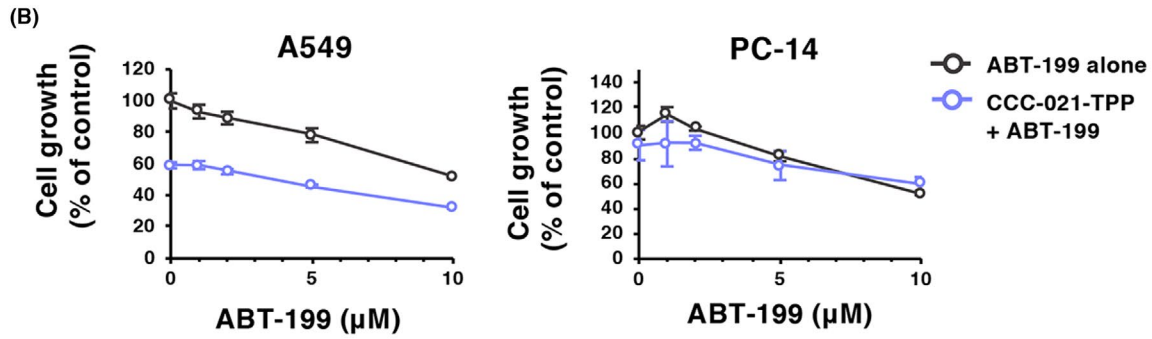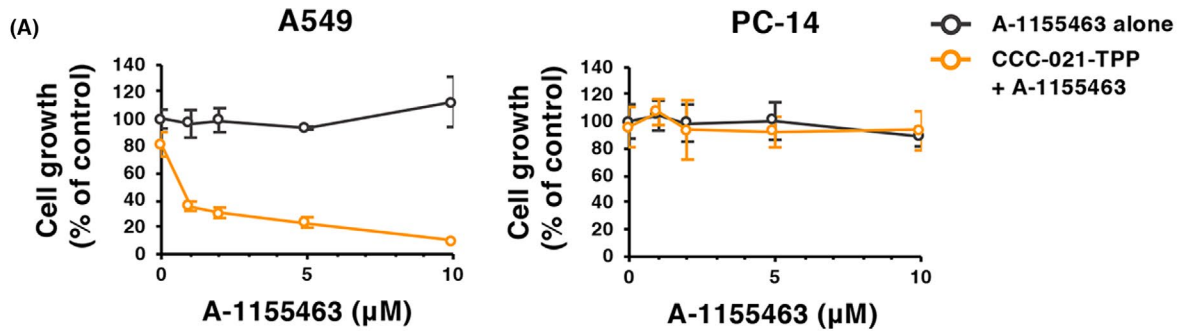
FIGURE 7 Induction of apoptosis by the combination of CCC-021-triphenylphosphonium (TPP) and A-1155463 in A549 cells. (A) Expression of poly(ADP-ribose) polymerase-1 (PARP-1), cleaved caspase-3, and γ-H2AX. Cells were treated with DMSO, 20 µM CCC-021-TPP alone, 4 µM A-1155463 alone, or their combination for 5 d. Uncropped western blot images are shown in Figure S12. (B) Annexin V/propidium iodide staining. Representative images were obtained by flow cytometry (top). Percentage of annexin V-positive cells (bottom). Cells were treated with DMSO, 20 µM CCC-021-TPP alone, 4 µM A-1155463 alone, or their combination for 4 d. C, Analysis of sub-G_1 fraction. Cells were treated with DMSO, 20 µM CCC-021-TPP alone, 4 µM A-1155463 alone, or their combination for 5 d. Cell cycle was analyzed by flow cytometry

4 | DISCUSSION

This study showed that CCC-021-TPP induced a decrease in *ND6* expression and complex I enzyme activity in A549 cells with 14582A > G mutation but not in PC-14 cells without the mutation. Accordingly, it increased mtROS generation and mitophagy exclusively in A549 cells. Thus, CCC-021-TPP showed its effects in a highly specific manner to the 14582G mutation. In general, linear-type PIPs are thought to be inferior to hairpin-type PIPs in DNA sequence recognition ability. However, we think that short, linear motifs of PIPs might show high mutation specificity in cases in targeting mtDNA because the mitochondrial genome is somewhat smaller in size than the nuclear genome, which could increase the specificity/off-target effect ratio. Intriguingly, CCC-021-TPP induced cellular senescence but not apoptosis in A549 cells. At present, it remains to be determined what the mechanisms are by which tumor cells undergo either apoptosis or senescence by the treatment with PIP-TPPs. It might be dependent on genetic background of target cells or the degree of suppression of the mitochondrial metabolism, bioenergetics, and surveillance arising from locations of, or the binding affinity of PIP-TPPs to, target mutations in mtDNA.

Although the precise mechanisms underlying CCC-021-TPP-induced cellular senescence in A549 cells remain uncertain, we observed an increase in LC3-II level, although bafilomycin A1 was required to suppress its turnover, and the retardation of cellular senescence by 3-MA in CCC-021-TPP-treated cells. These results suggested the involvement of autophagy/mitophagy in the senescence induction. Accumulating evidence indicates the relationship between autophagy and cellular senescence, but it is still inconclusive. Some studies reported that autophagy acted as a prosenescence mechanism.[35-39] Conversely, other studies reported that autophagy is negatively correlated with senescence.[40-42] With regard to mitophagy, it is reported to be reduced in senescent cells.[43] Thus, it seems likely that autophagy/mitophagy either increases or reduces cellular senescence in a context-dependent manner. We now think that in A549 cells mitophagy might be required to trigger senescence onset and subsequently reduced in later stages of senescence, which needs to be clarified in the future. Interestingly, in *Drosophila*, cell senescence occurred when mitochondrial dysfunction and RAS activation were simultaneously induced.[44] Because A549 cells carry the *KRAS* G12S mutation,[45] it is possible that mitochondrial dysfunction followed by stimulation of autophagy/mitophagy by CCC-021-TPP provokes cellular senescence.

The induction of BCL-XL appeared to be a cause of apoptosis resistance in CCC-021-TPP-treated A549 cells, which was supported by the fact that the combination of CCC-021-TPP and A-1155463 remarkably induced apoptosis. In addition to its well-known antiapoptotic role in preventing cytochrome c release,[46] BCL-XL is reported to be related to mitochondrial biogenetics; it modulates mitochondrial fusion and fission, increases total mitochondrial biomass, enhances the efficiency of the ATP synthesis by decreasing the proton leak within the F1F0 ATPase, and increases mitochondrial metabolism.[47,48] BCL-XL is also known to block autophagosome formation through binding to the autophagy regulator Beclin-1.[49] Furthermore, BCL-XL antagonizes mitophagy, dependent on Parkin, which ubiquitylates numerous outer mitochondrial membrane proteins and in turn recruits other proteins to initiate mitophagy.[50-52] Thus, from another point of view, overproduction of BCL-XL in CCC-021-TPP-treated A549 cells could reflect the self-defense mechanism to block excess autophagy/mitophagy, which ultimately leads to cell death.

Cellular senescence is not an irreversible form of growth arrest. Chemotherapy- or radiotherapy-induced senescence in tumor cells often re-enter a proliferative state and give rise to more aggressive progeny.[53] The SASP factors promote inflammatory responses and allow tumor cells' escape from immunosurveillance.[54,55] In this study, we detected an increase in IL-8 production, which is a neutrophil chemoattractant,[56] in CCC-021-TPP-treated A549 cells. Interleukin-6 is also known to stimulate cell proliferation, survival, invasiveness, and metastasis of tumor cells.[57] Thus, accumulation of induced senescence cells and chronic inflammation caused by SASP factors are undesirable outcomes of cancer therapy. As such, recent efforts have focused on the induction of cell death of senescent cells especially by small molecules (senolytics) that can selectively eliminate senescent tumor cells.[58-60] Our study showed the efficacy of ABT-263 as well as the BCL-XL-specific inhibitor A-1155463 to induce apoptosis in CCC-021-TPP-treated A549 cells.

Our in vivo studies showed that CCC-021-TPP was delivered to subcutaneous A549 tumors after intraperitoneal treatment as assessed by immunostaining for TPP. This is consistent with our previous report that PIPs can be delivered and retained in tumor tissues without any delivery reagents.[61] Notably, CCC-021-TPP treatment induced cellular senescence in the xenografted tumors. Indeed, a significant accumulation of neutrophils was observed in CCC-021-TPP-treated A549 tumors, probably reflecting increased IL-8 production from senescent A549 cells. Accumulating evidence shows that TANs can be classified into N1 and N2 TANs, the latter of which stimulate immunosuppression, tumor growth, angiogenesis, and metastasis.[56] Neutrophils accumulated in CCC-021-TPP-treated A549 tumors could be N2 TANs, which needs to be examined in the future. Consistent with the in vitro results, combined treatment of
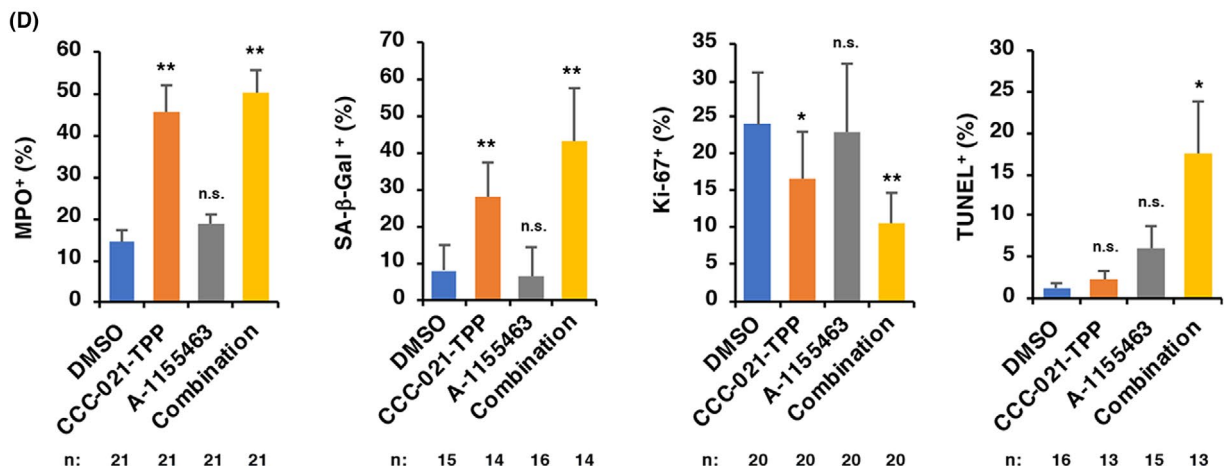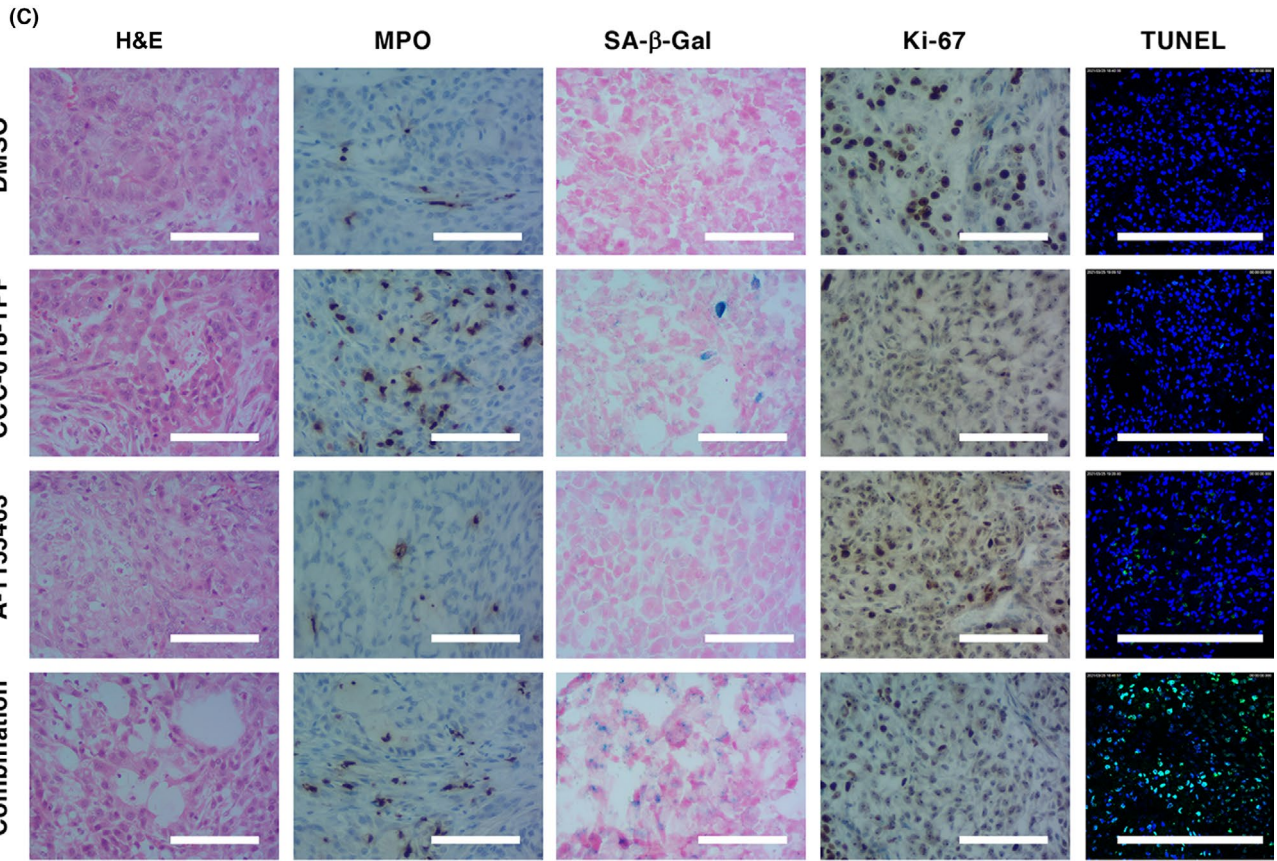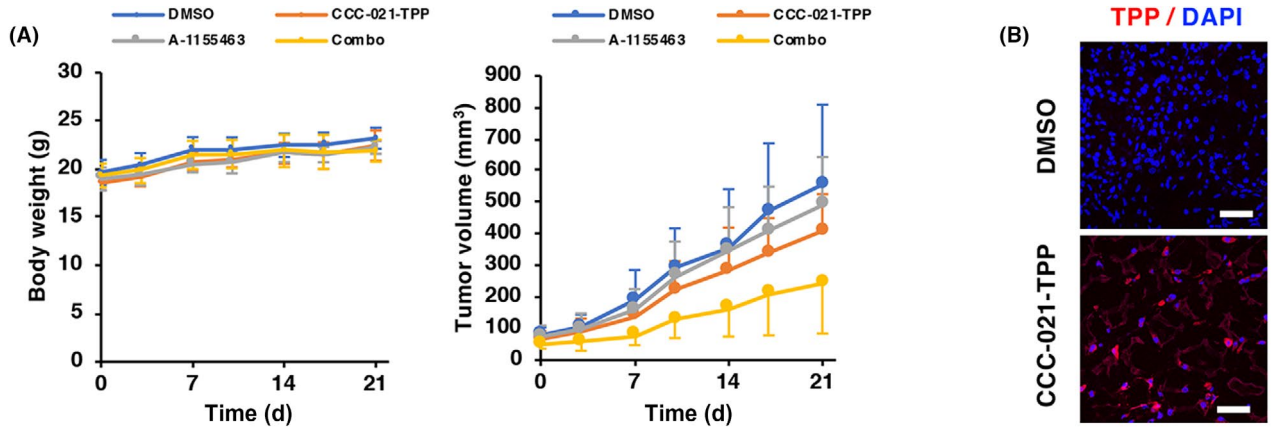
(A) Body weight and tumor volume graphs over time for DMSO, CCC-021-TPP, A-1155463, and Combo groups.

(B) TPP / DAPI immunofluorescence images for DMSO and CCC-021-TPP.

(C) H&E, MPO, SA-β-Gal, Ki-67, and TUNEL staining for DMSO, CCC-018-TPP, A-1155463, and Combination groups.

(D) Quantification bar graphs of MPO+ (%), SA-β-Gal+ (%), Ki-67+ (%), and TUNEL+ (%).

FIGURE 8 Suppression of A549 tumor growth by the combination of CCC-021-triphenylphosphonium (TPP) and A-1155463. A, Effects of intraperitoneal administration of indicated drugs on body weight (left) and tumor growth (right). n = 5 mice/group. Values are mean ± SD. (B) Immunostaining of tumor tissues from CCC-021-TPP-treated mice with anti-TPP Ab. C, Images of H&E staining, immunohistochemistry, and TUNEL staining of tumor tissues. Bar = 200 μm. (D) Percentage of myeloperoxidase (MPO)$^+$, senescence-associated β-galactosidase (SA-β-Gal)$^+$, Ki-67$^+$, and TUNEL$^+$ cells in tumor tissues calculated based on the number of nuclei in the field. Values are mean ± SD. *$P < .001$, **$P < .0001$ vs DMSO control. n, number of fields examined; n.s. not significant (one-way ANOVA and Tukey's test)

A549 tumors with CCC-021-TPP and A-1155463 markedly induced apoptosis. As a consequence, we observed the suppression of tumor growth by the combination without apparent body weight loss. These results clearly showed the effectiveness of therapy by the combination of CCC-021-TPP and A-1155463 against A549 tumors.

To date, no extensive study has determined how TPP-conjugated PIPs are distributed in various tissues in vivo. We found that, after repeated treatment, CCC-021-TPP could potentially accumulate in organs such as the lung, liver, and kidney, but curiously not the brain. Another interesting observation was the strong presence of TPP signal in Kupffer compared to parenchymal cells in the liver. As these cells are the resident macrophages in the sinusoidal lumen, the uptake of CCC-021-TPP from the bloodstream is possible. The low levels of CC3 in hepatic parenchymal cells and Kupffer cells also imply low hepatotoxicity of CCC-021-TPP. Kidney accumulation together with the low level in the lung might also indicate that clearance of excess CCC-021-TPP is likely through the kidney with urine. Although evidence of TPP signal in tubular epithelial cells, combined with residual signs of positive CC3 in tubular epithelial cells, could indicate some degree of nephrotoxicity, as tubular epithelium has the capacity to regenerate, repair, and re-epithelialize in response to a variety of insults,[62] overall nephrotoxicity could possibly be ameliorated. The lack of gross changes in tissue architecture (Figure S11) by H&E staining and no apparent change in body weight during 3 weeks of intraperitoneal therapy suggest that CCC-021-TPP is well tolerated in mice.

In conclusion, this study highlights the potential of mtDNA mutation-targeting PIP-TPPs to induce cellular senescence of certain tumor cells and, furthermore, to trigger apoptosis in combination with senolytic agents in vivo. An advantage of the use of PIP-TPPs targeting mtDNA mutations is their preferential binding to the mutant mtDNA over WT mtDNA. Therefore, unlike conventional DNA damaging agents that also induce senescence in certain tumor cells, mtDNA mutation-targeting PIP-TPPs can be used for cancer therapy, minimizing possible adverse effects. Further studies on such PIP-TPPs would give us valuable knowledge about their therapeutic potential against apoptosis-resistant and apoptosis-prone cancers.

ORCID

Jason Lin https://orcid.org/0000-0002-8086-3185
Hiroki Nagase https://orcid.org/0000-0002-3992-5399
Keizo Takenaga https://orcid.org/0000-0002-5341-6742

REFERENCES

1. Dervan PB. Design of sequence-specific DNA-binding molecules. *Science*. 1986;232:464-471. doi:10.1126/science.2421408
2. Dervan PB, Edelson BS. Recognition of the DNA minor groove by pyrrole-imidazole polyamides. *Curr Opi Struct Biol*. 2003;13:284-299. doi:10.1016/s0959-440x(03)00081-2
3. Kawamoto Y, Bando T, Sugiyama H. Sequence-specific DNA binding pyrrole-imidazole polyamides and their applications. *Bioorg Med Chem*. 2018;26:1393-1411. doi:10.1016/j.bmc.2018.01.026
4. Urbach AR, Dervan PB. Toward rules for 1:1 polyamide:DNA recognition. *Proc Natl Acad Sci U S A*. 2001;98:343-4348. doi:10.1073/pnas.081070798
5. Hiraoka K, Inoue T, Taylor RD, et al. Inhibition of KRAS codon 12 mutants using a novel DNA-alkylating pyrrole-imidazole polyamide conjugate. *Nat Commun*. 2015;6:6706. doi:10.1038/ncomms7706
6. Yoda H, Inoue T, Shinozaki Y, et al. Direct targeting of MYCN gene amplification by site-specific DNA alkylation in neuroblastoma. *Cancer Res*. 2019;79:830-840. doi:10.1158/0008-5472.CAN-18-1198
7. Krishnamurthy S, Yoda H, Hiraoka K, et al. Targeting the mutant PIK3CA gene by DNA-alkylating pyrrole-imidazole polyamide in cervical cancer. *Cancer Sci*. 2021;112:1141-1149. doi:10.1111/cas.14785
8. Koshikawa N, Yasui N, Kida Y, et al. A PI polyamide-TPP conjugate targeting a mtDNA mutation induces cell death of cancer cells with the mutation. *Cancer Sci*. 2021;112:504-2512. doi:10.1111/cas.14912
9. Nunnari J, Suomalainen A. Mitochondria: in sickness and in health. *Cell*. 2012;148:1145-1159. doi:10.1016/j.cell.2012.02.035

10. Scheid AD, Beadnell TC, Welch DR. Roles of mitochondria in the hallmarks of metastasis. *Br J Cancer*. 2021;124:124-135. doi:10.1038/s41416-020-01125-8

11. Ishikawa K, Imanishi H, Takenaga K, Hayashi J-I. Regulation of metastasis; mitochondrial DNA mutations have appeared on stage. *J Bioenerg Biomembr*. 2012;44:639-644. doi:10.1007/s10863-012-9468-6

12. Gonçalves VF. Mitochondrial genetics. *Adv Exp Med Biol*. 2019;1158:247-255. doi:10.1007/978-981-13-8367-0_13

13. Ishikawa K, Takenaga K, Akimoto M, et al. ROS-generating mitochondrial DNA mutations can regulate tumor cell metastasis. *Science*. 2008;320:661-664. doi:10.1126/science.1156906

14. Koshikawa N, Akimoto M, Hayashi J-I, Nagase H, Takenaga K. Association of predicted pathogenic mutations in mitochondrial ND genes with distant metastasis in NSCLC and colon cancer. *Sci Rep*. 2017;7:15535. doi:10.1038/s41598-017-15592-2

15. Takenaga K, Koshikawa N, Akimoto M, et al. MCT4 is induced by metastasis-enhancing pathogenic mitochondrial NADH dehydrogenase gene mutations and can be a therapeutic target. *Sci Rep*. 2021;11:13302. doi:10.1038/s41598-021-92772-1

16. Hashizume O, Shimizu A, Yokota N, et al. Specific mitochondrial DNA mutation in mice regulates diabetes and lymphoma development. *Proc Natl Acad Sci U S A*. 2012;109:10528-10533. doi:10.1073/pnas.1202367109

17. Kulawiec M, Owens KM, Singh KK. mtDNA G10398A variant in African-American women with breast cancer provides resistance to apoptosis and promotes metastasis in mice. *J Hum Genet*. 2009;54:647-654. doi:10.1038/jhg.2009.89

18. Kulawiec M, Owens KM, Singh KK. Cancer cell mitochondria confer apoptosis resistance and promote metastasis. *Cancer Biol Ther*. 2009;8(14):1378-1385. doi:10.4161/cbt.8.14.8751

19. Arnold RS, Sun CQ, Richards JC, et al. Mitochondrial DNA mutation stimulates prostate cancer growth in bone stromal environment. *Prostate*. 2009;6:1-11. doi:10.1002/pros.20854

20. Arnold RS, Fedewa SA, Goodman M, et al. Bone metastasis in prostate cancer: Recurring mitochondrial DNA mutation reveals selective pressure exerted by the bone microenvironment. *Bone*. 2015;78:81-86. doi:10.1016/j.bone.2015.04.046

21. Nunes JB, Peixoto J, Soares P, et al. OXPHOS dysfunction regulates integrin-β1 modifications and enhances cell motility and migration. *Hum Mol Genet*. 2015;24:1977-1990. doi:10.1093/hmg/ddu612

22. Lin YH, Chu YD, Lim SN, Chen CW, Yeh CT, Lin WR. Impact of an MT-RNR1 gene polymorphism on hepatocellular carcinoma progression and clinical characteristics. *Int J Mol Sci*. 2021;22:1119. doi:10.3390/ijms22031119

23. Zielonka J, Joseph J, Sikora A, et al. Mitochondria-targeted triphenylphosphonium-based compounds: Syntheses, mechanisms of action, and therapeutic and diagnostic applications. *Chem Rev*. 2017;117:10043-10120. doi:10.1021/acs.chemrev.7b00042

24. Koshikawa N, Kida Y, Yasui N, et al. A linear five-ring pyrrole-imidazole polyamide-Triphenylphosphonium conjugate targeting a mitochondrial DNA mutation efficiently induces apoptosis of HeLa cybrid cells carrying the mutation. *Biochem Biophys Res Commun*. 2021;576:93-99. doi:10.1016/j.bbrc.2021.08.088

25. Yuan Y, Wang W, Li H, et al. Nonsense and missense mutation of mitochondrial ND6 gene promotes cell migration and invasion in human lung adenocarcinoma. *BMC Cancer*. 2015;15:346. doi:10.1186/s12885-015-1349-z

26. Tokunaga K, Nakamura Y, Sakata K, et al. Enhanced expression of a glyceraldehyde-3-phosphate dehydrogenase gene in human lung cancers. *Cancer Res*. 1987;47:5616-5619.

27. Akimoto M, Iizuka M, Kanematsu R, Yoshida M, Takenaga K. Anticancer effect of ginger extract against pancreatic cancer cells

28. mainly through reactive oxygen species-mediated autotic cell death. *PLoS One*. 2015;10:e0126605. doi:10.1371/journal.pone.0126605

28. Percie du Sert N, Ahluwalia A, Alam S, et al. Reporting animal research: Explanation and elaboration for the ARRIVE guidelines 2.0. *PLoS Biol*. 2020;18:e3000411. doi:10.1371/journal.pbio.3000411

29. Pickles S, Vigié P, Youle RJ. Mitophagy and quality control mechanisms in mitochondrial maintenance. *Curr Biol*. 2018;28:R170-R185. doi:10.1016/j.cub.2018.01.004

30. Mauvezin C, Neufeld TP. Bafilomycin A1 disrupts autophagic flux by inhibiting both V-ATPase-dependent acidification and Ca-P60A/SERCA-dependent autophagosome-lysosome fusion. *Autophagy*. 2015;11:1437-1438. doi:10.1080/15548627.2015.1066957

31. Kubo A, Nakagawa K, Varma RK, et al. The p16 status of tumor cell lines identifies small molecule inhibitors specific for cyclin-dependent kinase 4. *Clin Cancer Res*. 1999;5:4279-4286.

32. Lopes-Paciencia S, Saint-Germain E, Rowell MC, Ruiz AF, Kalegari P, Ferbeyre G. The senescence-associated secretory phenotype and its regulation. *Cytokine*. 2019;117:15-22. doi:10.1016/j.cyto.2019.01.013

33. Ito S, Koshikawa N, Mochizuki S, Takenaga K. 3-Methyladenine suppresses cell migration and invasion of HT1080 fibrosarcoma cells through inhibiting phosphoinositide 3-kinases independently of autophagy inhibition. *Int J Oncol*. 2007;31:261-268.

34. Wang H, Jiang T, Li W, Gao N, Zhang T. Resveratrol attenuates oxidative damage through activating mitophagy in an in vitro model of Alzheimer's disease. *Toxicol Lett*. 2018;282:100-108. doi:10.1016/j.toxlet.2017.10.021

35. Young AR, Narita M, Ferreira M, et al. Autophagy mediates the mitotic senescence transition. *Genes Dev*. 2009;23:798-803. doi:10.1101/gad.519709

36. Goehe RW, Di X, Sharma K, et al. The autophagy-senescence connection in chemotherapy: must tumor cells (self) eat before they sleep? *J Pharmacol Exp Ther*. 2012;343:763-778. doi:10.1124/jpet.112.197590

37. Qi M, Fan S, Yao G, et al. Pseudolaric acid B-induced autophagy contributes to senescence via enhancement of ROS generation and mitochondrial dysfunction in murine fibrosarcoma L929 cells. *J Pharmacol Sci*. 2013;121:200-211. doi:10.1254/jphs.12269fp

38. Bernard M, Yang B, Migneault F, et al. Autophagy drives fibroblast senescence through MTORC2 regulation. *Autophagy*. 2020;16:2004-2016. doi:10.1080/15548627.2020.1713640

39. Polewska J, Skwarska A, Augustin E, Konopa J. DNA-damaging imidazoacridinone C-1311 induces autophagy followed by irreversible growth arrest and senescence in human lung cancer cells. *J Pharmacol Exp Ther*. 2013;346:393-405. doi:10.1124/jpet.113.203851

40. Kang HT, Lee KB, Kim SY, Choi HR, Park SC. Autophagy impairment induces premature senescence in primary human fibroblasts. *PLoS One*. 2011;6:e23367. doi:10.1371/journal.pone.0023367

41. Tai H, Wang Z, Gong H, et al. Autophagy impairment with lysosomal and mitochondrial dysfunction is an important characteristic of oxidative stress-induced senescence. *Autophagy*. 2017;13:99-113. doi:10.1080/15548627.2016.1247143

42. García-Prat L, Martínez-Vicente M, Perdiguero E, et al. Autophagy maintains stemness by preventing senescence. *Nature*. 2016;529:37-42. doi:10.1038/nature16187

43. Korolchuk VI, Miwa S, Carroll B, von Zglinicki T. Mitochondria in cell senescence: Is mitophagy the weakest link? *EBioMedicin*. 2017;21:7-13. doi:10.1016/j.ebiom.2017.03.020

44. Nakamura M, Ohsawa S, Igaki T. Mitochondrial defects trigger proliferation of neighbouring cells via a senescence-associated secretory phenotype in Drosophila. *Nat Commun*. 2014;5:5264. doi:10.1038/ncomms6264

45. Moran DM, Trusk PB, Pry K, Paz K, Sidransky D, Bacus SS. KRAS mutation status is associated with enhanced dependency on folate

metabolism pathways in non-small cell lung cancer cells. *Mol Cancer Ther.* 2014;13:1611-1624. doi:10.1158/1535-7163.MCT-13-0649

46. Jonas EA, Porter GA, Alavian KN. BCL-xL in neuroprotection and plasticity. *Front Physiol.* 2014;5:355. doi:10.3389/fphys.2014.00355

47. Borrás C, Mas-Bargues C, Román-Domínguez A, et al. BCL-XL, a mitochondrial protein involved in successful aging: From C. elegans to human centenarians. *Int J Mol Sci.* 2020;21(2):418. doi:10.3390/ijms21020418

48. Alavian KN, Li H, Collis L, et al. Bcl-xL regulates metabolic efficiency of neurons through interaction with the mitochondrial F1FO ATP synthase. *Nat Cell Biol.* 2011;13:1224-1233. doi:10.1038/ncb2330

49. Noble CG, Dong JM, Manser E, Song H. Bcl-xL and UVRAG cause a monomer-dimer switch in Beclin1. *J Biol Chem.* 2008;283:26274-26282. doi:10.1074/jbc.M804723200

50. Zhou F, Yang Y, Xing D. Bcl-2 and Bcl-xL play important roles in the crosstalk between autophagy and apoptosis. *FEBS J.* 2011;278:403-413. doi:10.1111/j.1742-4658.2010.07965.x

51. Hollville E, Carroll RG, Cullen SP, Martin SJ. Bcl-2 family proteins participate in mitochondrial quality control by regulating Parkin/PINK1-dependent mitophagy. *Mol Cell.* 2014;55:451-466. doi:10.1016/j.molcel.2014.06.001

52. Jin SM, Youle RJ. PINK1- and Parkin-mediated mitophagy at a glance. *J Cell Sci.* 2012;125:795-799. doi:10.1242/jcs.093849

53. Saleh T, Bloukh S, Carpenter VJ, et al. Therapy-induced senescence: An "old" friend becomes the enemy. *Cancers (Basel).* 2020;12:822. doi:10.3390/cancers12040822

54. Muñoz D, Yannone SM, Daemen A, et al. Targetable mechanisms driving immunoevasion of persistent senescent cells link chemotherapy-resistant cancer to aging. *JCI Insight.* 2019;5:e124716. doi:10.1172/jci.insight.124716

55. Pereira BI, Devine OP, Vukmanovic-Stejic M, et al. Senescent cells evade immune clearance via HLA-E-mediated NK and CD8+ T cell inhibition. *Nat Commun.* 2019;10:2387. doi:10.1038/s41467-019-10335-5

56. Masucci MT, Minopoli M, Carriero MV. Tumor associated neutrophils. Their role in tumorigenesis, metastasis, prognosis and therapy. *Front Oncol.* 2019;9:1146. doi:10.3389/fonc.2019.01146

57. Johnson DE, O'Keefe RA, Grandis JR. Targeting the IL-6/JAK/STAT3 signalling axis in cancer. *Nat Rev Clin Oncol.* 2018;15:234-248. doi:10.1038/nrclinonc.2018.8

58. Short S, Fielder E, Miwa S, von Zglinicki T. Senolytics and senostatics as adjuvant tumour therapy. *EBioMedicine.* 2019;41:683-692. doi:10.1016/j.ebiom.2019.01.056

59. Chang J, Wang Y, Shao L, et al. Clearance of senescent cells by ABT263 rejuvenates aged hematopoietic stem cells in mice. *Nat Med.* 2016;22:78-83. doi:10.1038/nm.4010

60. Saleh T, Carpenter VJ, Tyutyunyk-Massey L, et al. Clearance of therapy-induced senescent tumor cells by the senolytic ABT-263 via interference with BCL-XL -BAX interaction. *Mol Oncol.* 2020;14:2504-2519. doi:10.1002/1878-0261.12761

61. Inoue T, Shimozato O, Matsuo N, et al. Hydrophobic structure of hairpin ten-ring pyrrole-imidazole polyamides enhances tumor tissue accumulation/retention in vivo. *Bioorg Med Chem.* 2018;26:2337-2344. doi:10.1016/j.bmc.2018.03.029

62. Maeshima A, Takahashi S, Nakasatomi M, Nojima Y. Diverse cell populations involved in regeneration of renal tubular epithelium following acute kidney injury. *Stem Cells Int.* 2015;2015:964849. doi:10.1155/2015/964849

SUPPORTING INFORMATION

Additional supporting information may be found in the online version of the article at the publisher's website.